
THE UNIVERSITY OF ARIZONA
University Libraries
UA CAMPUS
REPOSITORY

Microchannel plate detector technology potential for LUVOIR and HabEx

Item Type	Article
Authors	Schindhelm, Eric R.; Green, J. C.; Siegmund, Oswald H. W.; Ertley, Camden; Fleming, Brian T.; France, Kevin C.; Harris, Walter M.; Harwit, Alex; McCandliss, Stephan R.; Vallerga, John V.
Citation	O. H. W. Siegmund, C. Ertley, J. V. Vallerga, E. R. Schindhelm, A. Harwit, B. T. Fleming, K. C. France, J. C. Green, S. R. McCandliss, W. M. Harris, "Microchannel plate detector technology potential for LUVOIR and HabEx", Proc. SPIE 10397, UV, X-Ray, and Gamma-Ray Space Instrumentation for Astronomy XX, 1039711 (29 August 2017); doi: 10.1117/12.2274281; http://dx.doi.org/10.1117/12.2274281
DOI	10.1117/12.2274281
Publisher	SPIE-INT SOC OPTICAL ENGINEERING
Journal	UV, X-RAY, AND GAMMA-RAY SPACE INSTRUMENTATION FOR ASTRONOMY XX
Rights	© 2017 SPIE.
Download date	26/08/2022 16:02:42
Item License	http://rightsstatements.org/vocab/InC/1.0/
Version	Final published version
Link to Item	http://hdl.handle.net/10150/626502

PROCEEDINGS OF SPIE

SPIEDigitalLibrary.org/conference-proceedings-of-spie

Microchannel plate detector technology potential for LUVOIR and HabEx

O. H. W. Siegmund, C. Ertley, J. V. Vallerga, E. R. Schindhelm, A. Harwit, et al.

O. H. W. Siegmund, C. Ertley, J. V. Vallerga, E. R. Schindhelm, A. Harwit, B. T. Fleming, K. C. France, J. C. Green, S. R. McCandliss, W. M. Harris, "Microchannel plate detector technology potential for LUVOIR and HabEx," Proc. SPIE 10397, UV, X-Ray, and Gamma-Ray Space Instrumentation for Astronomy XX, 1039711 (29 August 2017); doi: 10.1117/12.2274281

SPIE.

Event: SPIE Optical Engineering + Applications, 2017, San Diego, California, United States

Downloaded From: https://www.spiedigitallibrary.org/conference-proceedings-of-spie on 1/29/2018 Terms of Use: https://www.spiedigitallibrary.org/terms-of-use

Microchannel Plate Detector Technology Potential for LUVOIR and HabEx

O.H.W. Siegmund[a], C. Ertley[a], J.V. Vallerga[a], E.R. Schindhelm[b], A. Harwit[b], B.T. Fleming[c], K.C. France[c], J.C. Green[c], S.R. McCandliss[d], W.M. Harris[e],

[a]Space Sciences Laboratory, 7 Gauss Way, University of California, Berkeley, CA 94720
[b]Ball Aerospace & Technologies Corp. 1600 Commerce St, Boulder, CO 80301
[c] University of Colorado, 1234 Innovation Dr. Boulder, CO 80303
[d]The Johns Hopkins University, 3400 N. Charles Street, Baltimore, MD 21218
[e]LPL, University of Arizona, 1629 E. University Blvd. Tucson, AZ 85721

ABSTRACT

Microchannel plate (MCP) detectors have been the detector of choice for ultraviolet (UV) instruments onboard many NASA missions. These detectors have many advantages, including high spatial resolution (<20 μm), photon counting, radiation hardness, large formats (up to 20 cm), and ability for curved focal plane matching. Novel borosilicate glass MCPs with atomic layer deposition combine extremely low backgrounds, high strength, and tunable secondary electron yield. GaN and combinations of bialkali/alkali halide photocathodes show promise for broadband, higher quantum efficiency. Cross-strip anodes combined with compact ASIC readout electronics enable high spatial resolution over large formats with high dynamic range. The technology readiness levels of these technologies are each being advanced through research grants for laboratory testing and rocket flights. Combining these capabilities would be ideal for UV instruments onboard the Large UV/Optical/IR Surveyor (LUVOIR) and the Habitable Exoplanet Imaging Mission (HABEX) concepts currently under study for NASA's Astrophysics Decadal Survey.

Keywords: Microchannel Plate, Imaging, Photon Counting.

1. INTRODUCTION

Photon counting, imaging microchannel plate (MCP) sensors are widely used in astronomy, high energy physics and remote sensing applications[1-8]. Sensing of photons, charged particles, and neutrons can be accomplished using high detection efficiency photocathodes[8] in open faced detectors (< 110nm range) or in ultra-high vacuum sealed tube devices (>110nm range). In response to the upcoming decadal survey in 2020 several initiatives are being examined as future NASA observatories. Amongst these are the Large UV/Optical/Infrared Surveyor (LUVOIR) and the Habitable Exoplanet Imaging Mission (HABEX). Those efforts are complemented by studies of new mid-range missions called "Probes". Cosmic Evolution Through UV Spectroscopy (CETUS), a Probe mission currently selected for study, is a UV/optical counterpart to these observatory missions.

Both the LUVOIR and HABEX mission concepts plan to have a suite of instruments to perform multi-wavelength observations. LUVOIRs science goals include, but are not limited to, epoch of reionization, through galaxy formation and evolution, star and planet formation, solar system remote sensing, and exoplanet characterization. The main goal of HabEx is to directly image planetary systems around Sun-like stars, but plans to have the capability to perform a broad range of general astrophysics studies. The CETUS mission concept will combine a 1.5 m aperture, wide field of view telescope with UV detectors for imaging and spectroscopic surveys to address a variety of topics in

UV, X-Ray, and Gamma-Ray Space Instrumentation for Astronomy XX, edited by Oswald H. Siegmund,
Proc. of SPIE Vol. 10397, 1039711 · © 2017 SPIE · CCC code: 0277-786X/17/$18 · doi: 10.1117/12.2274281

Downloaded From: https://www.spiedigitallibrary.org/conference-proceedings-of-spie on 1/29/2018 Terms of Use: https://www.spiedigitallibrary.org/terms-of-use

cosmic origins. All of these instruments will require sensitive large-format UV detectors with high spatial resolution, low noise performance, and high dynamic range to achieve their scientific goals.

Current baseline for the LUVOIR Multi-Object Spectrograph (LUMOS) are 200×200 mm^2 MCP detectors with cross strip (XS) anodes. MCPs have the advantage of a rich flight heritage and good performance characteristics, including extremely low background with zero read noise, large areas with the ability to curve for focal plane matching, "solar blind" photocathodes, and are insensitive to high radiation environments. Improvements still need to be made to the dynamic range and the UV detection efficiency in addition to further enhancements of the processing electronics. A full detector requirement list for the multi-object spectrometer and imager is shown in Table 1.

Table 1.

LUMOS Imager	
Number of MCPs	1
Spectral Range	1000 – 2000 Å
Plate Type	Borosilicate
Cathode	CsI
Anode	Cross Strip
Size	200×200
Resol Size	20 μm
Digital Pixel Size	$\lesssim 5$ μm
Curvature	Biconic
Radius	$R_x = 1200$ mm, $R_y = 16{,}000$ mm
Desired Global Count Rate	10 Mhz
Desired Local Count Rate	$\gtrsim 100$ hz resol^{-1}

LUMOS FUV MOS	
Number of Channels	4 in a 2×2 tiling
Spectral Range	1000 – 2000 Å
Plate Type	Borosilicate
Cathode	2× CsI, 2× Bialkali
Anode	Cross Strip
Size (Each)	200×200
Maximum Active Area Gap	12 mm Between Channels
Resol Size	20 μm
Digital Pixel Size	$\lesssim 5$ μm
Curvature	Cylindrical about x-dispersion axis
Radius (Full Array)	1820 mm
Desired Global Count Rate	10 Mhz (per Channel)
Desired Local Count Rate	$\gtrsim 100$ hz resol^{-1}

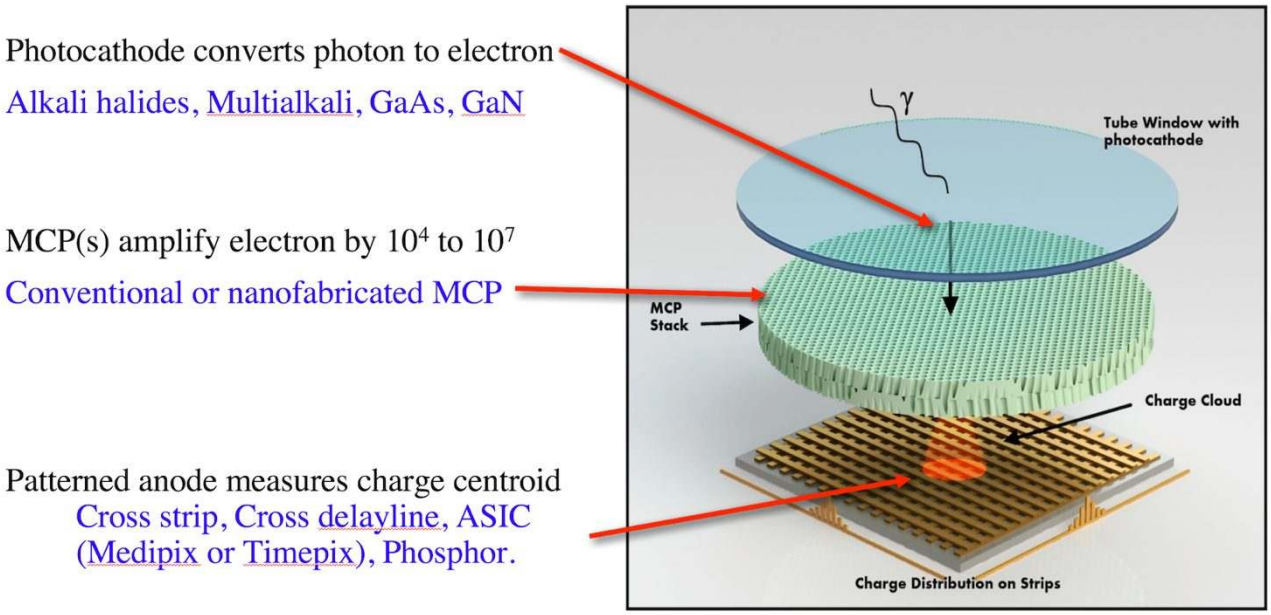

Figure 1. MCP cross strip imaging sensor. A photocathode is deposited on a window or on a pair of MCPs. Emitted photoelectrons are detected/multiplied by MCPs and collected by several strips in each axis to encode X,Y positions.

2. MCP DETECTORS AND READOUTS

A schematic of an MCP detector scheme is shown in Fig. 1. In this device, the radiation passes through the input window and is converted to photoelectrons by a photocathode. The window is used for ultra-high vacuum sealed tube devices where the photocathode can be deposited on the window as a semitransparent layer, and/or on the top of the front MCP as an opaque layer. Below wavelengths of

Downloaded From: https://www.spiedigitallibrary.org/conference-proceedings-of-spie on 1/29/2018 Terms of Use: https://www.spiedigitallibrary.org/terms-of-use

~110 nm a window cannot be used and these devices are made "open-faced". The emitted photoelectrons from the photocathode are amplified by a pair, or triplet, of MCPs and then detected by a readout anode. The latter can take many forms, however, we have significant efficacy with readouts that are patterns of conductive strips in both the X and Y directions. Determination of the single event X and Y positions can be achieved with pulse arrival time differences at the end of delay lines (cross delay line (XDL) anodes[4]) or from the centroid of the charge footprint sampled by a cross strip anode (XS)[9,10]. Time tagging of events to < 100 ps[1,11], and position resolution < 20 μm[3,9,12] can be achieved with such readouts. Background rates can be exceeding low (<0.05 events cm^{-2} sec^{-1})[13], MCPs are inherently radiation hard and have low sensitivity to gamma ray flux[14].

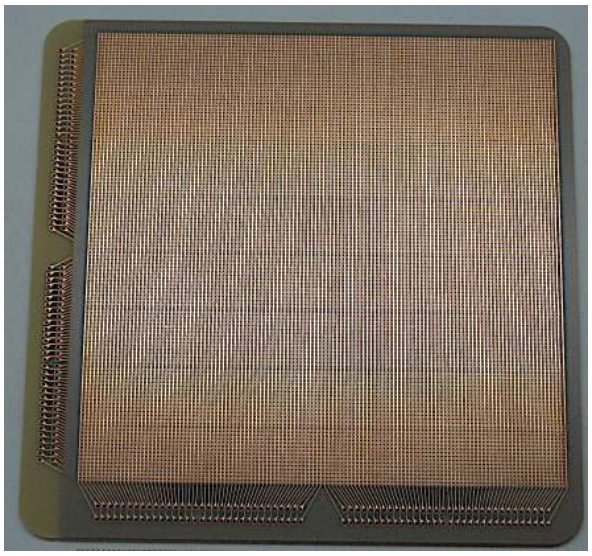

Figure 2. Cross strip anode having 95 x 95mm format with 128 strips in each axis to sample the MCP charge cloud distributions.

Figure 3. Cross strip detector with ~95 x 95mm aperture. Four 64 channel preamplifiers are shown attached to the detector.

Electronic readout MCP sensors have been used as photon counting, imaging, event time tagging detectors for a number of astronomical[8,15,16], remote sensing[17], time resolved biological imaging[18], photoelectron emission spectroscopy[1] and night time sensing[19] applications. The development of large area, high performance, photon counting, imaging, timing detectors also has significance for "open faced" configurations for UV and particle detection in space astrophysics, mass spectroscopy and many time-of–flight applications. Furthermore, sealed tube configurations for optical/UV sensing also have applications in detection of Cherenkov light (RICH), scintillation detection, and neutron imaging applications[20]. Cross strip readouts are of particular interest since they have the capability to be scaled for the largest format detectors and generally have best spatial resolution and highest event rate handling capability. The largest XS detector to date is ~100 mm format[21], a typical XS anode (95 mm) is shown in Fig. 2. The latter was incorporated into a detector system (Fig. 3) with a pair of MCPs with 8 μm pores and 4 × 64 channel amplifiers with downstream ADC/FPGA's (Xilinx Virtex 6) giving ~18 μm spatial resolution at rates up to 5 MHz.

3. ATOMIC LAYER MCPS USING BOROSILICATE SUBSTRATES

3.1. Borosilicate microcapillary arrays with ALD functionalization

Amplification of single particle or photon events using "standard" MCPs to multiply the primary emitted electrons has been accomplished with lead glass microcapillary arrays[6]. Until recently there

Downloaded From: https://www.spiedigitallibrary.org/conference-proceedings-of-spie on 1/29/2018 Terms of Use: https://www.spiedigitallibrary.org/terms-of-use

has been no "major" change to this method of producing MCPs for decades. Nano-fabrication using atomic layer deposition (ALD) on borosilicate microcapillary arrays offer a completely new way to build MCPs. The initial fabrication steps parallel conventional MCPs, but use inexpensive hollow borosilicate tube arrays (Fig. 4) with no need to remove a core glass. Resistive and then secondary emissive layers are deposited using the ALD process[22] and final contact electrodes are applied thereafter. The borosilicate substrate (Fig. 5) has a high glass softening temperature (>700 °C) allowing various unconventional processes to be accomplished with these MCPs.

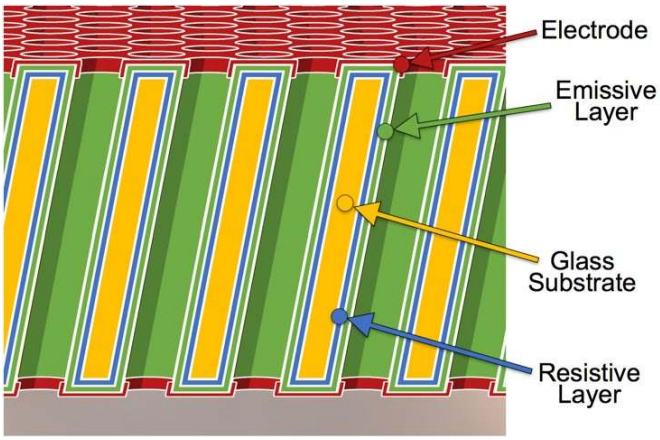

Figure 4. Borosilicate glass substrates are functionalized with atomic layer depositions. The resistive layer is covered with high secondary emission (Al_2O_3 or MgO) material, & NiCr electrodes.

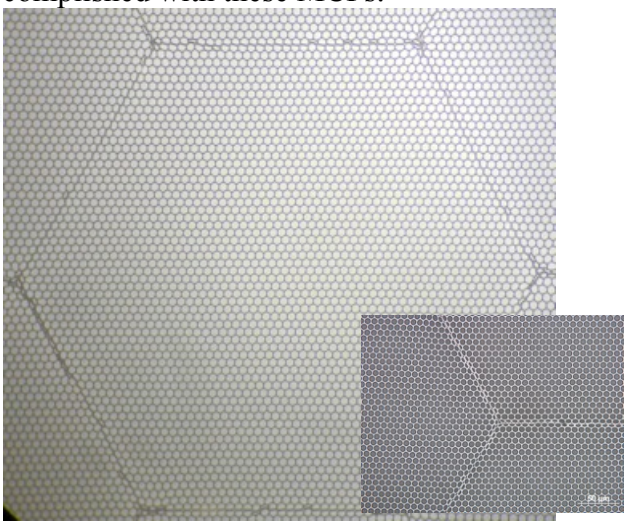

Figure 5. Photo of a 20µm pore C14 substrate with better than 1µm pore uniformity and low multi-fiber boundary distortions 74% open area, 60:1 L/D. Inset – 6µm pore substrate, 65% OAR.

The ALD process significantly reduces the MCP outgassing which has a direct effect on MCP detector lifetimes[23]. Borosilicate microcapillary substrates have been fabricated by Incom Inc. in two compositions, C5 and C14, with C14 now adopted as the standard. Pore sizes of 40 µm, 20 µm, 10 µm, and 6 µm have been made with pore length to diameter (L/d) ratios of 80:1, 60:1 and 40:1 and bias angles 8° and 13°. Substrate sizes range from 25 mm circular to 200 mm square. The open area fraction is nominally 74%, but has been made up to 83%. High secondary emissive layers of Al_2O_3 or MgO have both been used, and MCP resistances are within conventional ranges. The quality and uniformity of the ALD MCP substrates has improved greatly during development and now arrays with pores as small as 6 µm are being made.

Representative gain vs voltage curves for Al_2O_3 coated ALD C14 substrate MCPs are shown in Fig. 6 and demonstrate gain values comparable to standard lead glass MCPs[6,24]. MgO coated ALD MCPs give similar values. We compare the pulse amplitude distributions at several gain values for triple stacks of ALD MCPs to those for conventional MCPs in Fig. 7. With the high secondary emission coefficient of MgO we get better multiplication and this results in tighter saturated pulse amplitude distributions. This is very useful for event discrimination and reduction of signal dynamic range in application with modern low gain imaging detector readout schemes. The robustness of the ALD and substrate material has also proven advantageous in achievement of high local event rate capacity. This requires lower MCP resistance to support short recharge times, which is possible with C14 material with significantly reduced risk of thermal runaway compared to conventional MCPs. Local rates approaching 1 kHz per pore with acceptable gain droop have been achieved (Fig. 8) with low resistance ALD MCPs even at fairly high gain (5×10^6). At nominal gain (~1×10^6) for XS detectors the achievable rates would be proportionally higher.

Downloaded From: https://www.spiedigitallibrary.org/conference-proceedings-of-spie on 1/29/2018 Terms of Use: https://www.spiedigitallibrary.org/terms-of-use

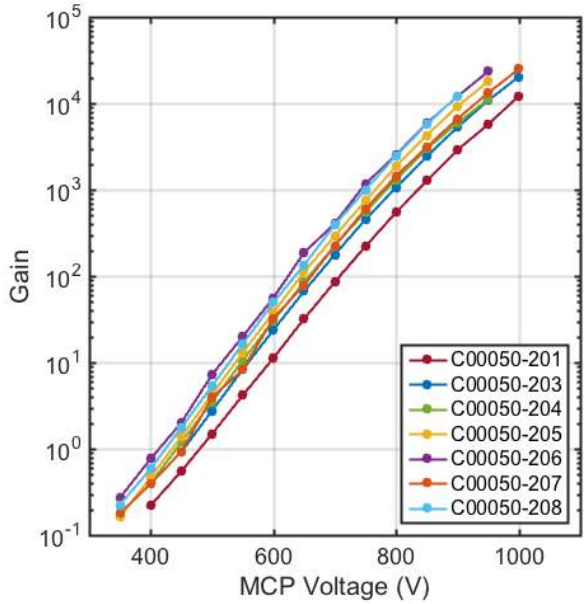

Fig. 6. Gain characteristics of 33 mm diameter Al_2O_3 coated C14 substrate MCPs, 20 µm pore, 74% open area, 60:1 L/D, 8° bias angle.

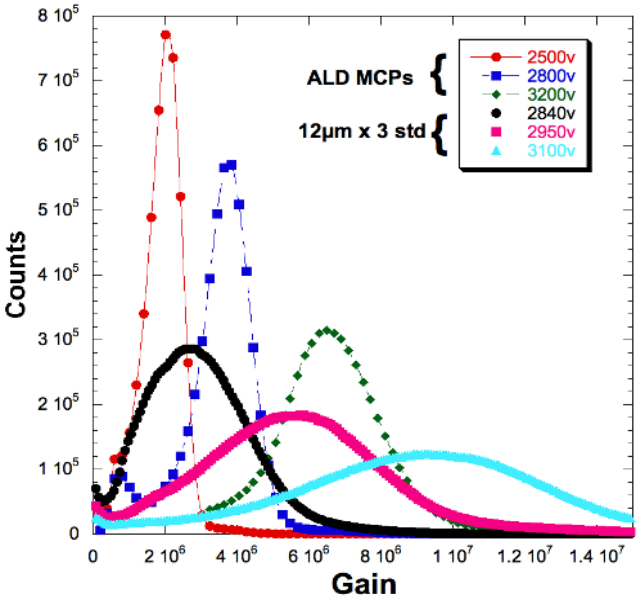

Fig. 7: Pulse height distributions for ALD MCPs are narrower than standard 12µm pore MCPs. ALD MCP triplet (33 mm, 20 µm pore, 60:1 L/d, 8° bias) with MgO emissive layer.

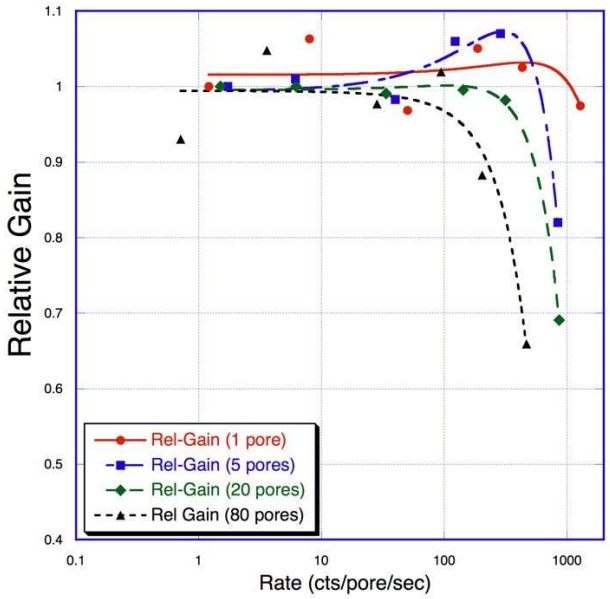

Figure 8. Gain stability for high local rates up to kHz / pore for a low resistance (8 MΩ) ALD 33 mm MCP pair at ~5 × 10^6 gain. 10 µm pores, 8° bias angle, 74% open area ratio, 80:1 L/D.

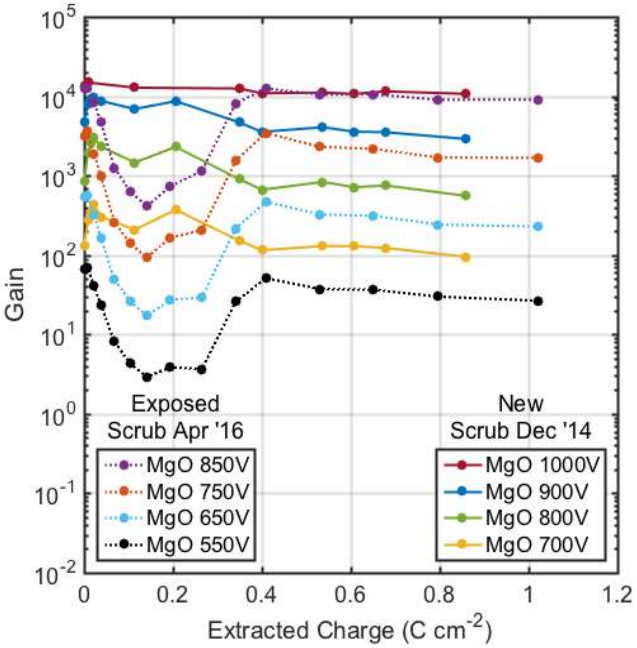

Figure 9. Burn-in (scrub) of C14 MgO coated ALD MCPs with 20 µm pores, 8° bias angle, 74% open area ratio, 60:1 L/D show excellent gain stability when new. After prolonged storage, they show a gain "dip" and then recover to the initial gain levels.

3.2. Borosilicate ALD MCP Preconditioning and Lifetime Characteristics

The lifetime and preconditioning of ALD MCPs is significantly different than conventional MCPs [25]. The secondary emissive MgO or Al_2O_3 layer for ALD MCPs is the most important factor for the behavior of the stability of ALD MCPs. Al_2O_3 shows a decrease in the secondary emission coefficient during surface cleaning[26]. We have seen that the gain drops on Al_2O_3 coated MCPs during high current

Downloaded From: https://www.spiedigitallibrary.org/conference-proceedings-of-spie on 1/29/2018 Terms of Use: https://www.spiedigitallibrary.org/terms-of-use

"burn-in", but the total charge extraction for stabilization is smaller than for standard MCPs[27]. However, there is an increase in MgO secondary emission coefficient during surface cleaning[26]. With early (C5) devices we have seen significant increases (×10) in MgO ALD MCP gain when subjected to a 350 °C vacuum bake. Subsequently "burn-in" with a high flux at low overall gain showed no gain change at normal operational settings (2×10^6) after 7 C cm^{-2} extracted[25]. Recent MgO ALD C14 MCPs show virtually no gain change during burn-in straight "out of the box" (Fig. 9). This may be attributable to better MgO cleanliness, which is supported by further data on MgO ALD MCPs from the same batch. These were stored in air for over a year, and showed initial gain decrease, but subsequently recovered to full gain[17]. These observations offer a unique advancement in MCP operational stability using MgO ALD C14 MCPs implemented for LUVOIR and other missions.

3.3. ALD MCP Background Event Characteristics

Reduction of background signal is as important as having high QE for low signal to noise observations. The background event for conventional MCPs is ~0.25 events cm^{-2} sec^{-1} and is dominated by ^{40}K beta decay in the MCP glass[5]. The low intrinsic radioactivity of the C5 and C14 glass compositions results in MCP background much lower (<0.05 events cm^{-2} sec^{-1}) than conventional MCPs[13]. Pulse amplitude distributions for UV and background events for a pair of MgO coated ALD borosilicate substrate MCPs are shown in Fig. 10. The UV shows peaked distributions and negative exponential distributions for background events that are generated throughout the bulk of the MCP material. We expect ~0.02 events cm^{-2} sec^{-1} for muon detections[5]. The background event image distribution is uniform (Fig. 11) even for 20 cm ALD MCPs, with a low incidence of "warm spots" due to debris. Another important factor is background induced by "in-orbit" high energy events.

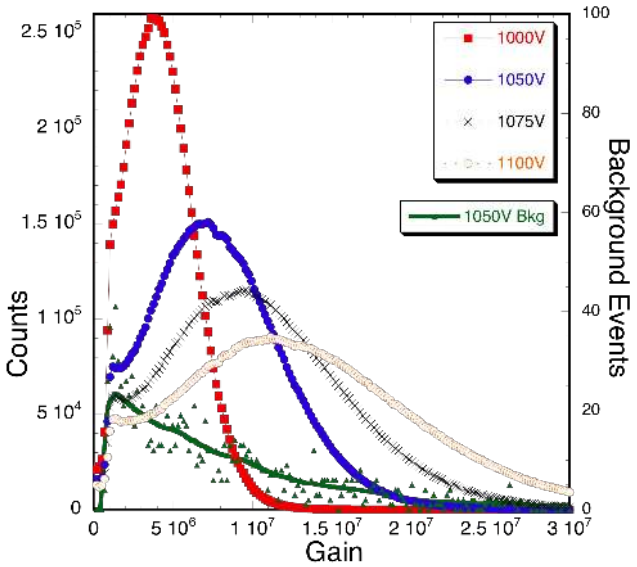

Figure 10. Pulse amplitude distributions for a 33mm diameter ALD MCP pair with 20 µm pore borosilicate substrate, 60:1 L/d, 8° bias, 254 nm UV and 3000 sec background distributions.

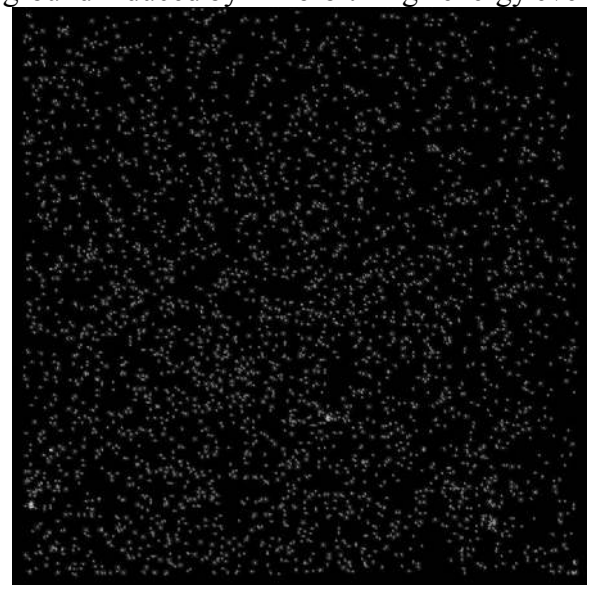

Figure 11. Background event image accumulation (500 sec) for a 20 x 20 cm, 60:1 L/d ALD borosilicate MCP pair, 8° bias. 0.7 mm pair gap at 200v bias, gain ~7 x 10^6, 0.028 events cm^{-2} sec^{-1}.

In Figs. 12 and 13 we compare pulse amplitude distributions and detection rates for conventional and ALD MCPs. For MeV Gamma radiation, the ALD MCPs are about a factor of 2.5 lower efficiency (0.8%) than conventional MCPs (Figs. 12, 13). This is a result of the absence of lead in the C5/C14 glasses. For MeV Beta radiation, the efficiency is the same (~25%) for both MCP types since the cross sections are similar. However, the charged particle background can be reduced by the use of a

Downloaded From: https://www.spiedigitallibrary.org/conference-proceedings-of-spie on 1/29/2018 Terms of Use: https://www.spiedigitallibrary.org/terms-of-use

coincidence shield as was done for the EURD instrument. Fast timing (20 ns) of signals at the detector compared to the scintillator allow high energy events to be rejected at up to 85% efficiency[28]. Rejecting high amplitude events above the UV photon gain limit would also help. An estimate of the final background rate suggests values less than 0.03 events cm^{-2} sec^{-1} are achievable.

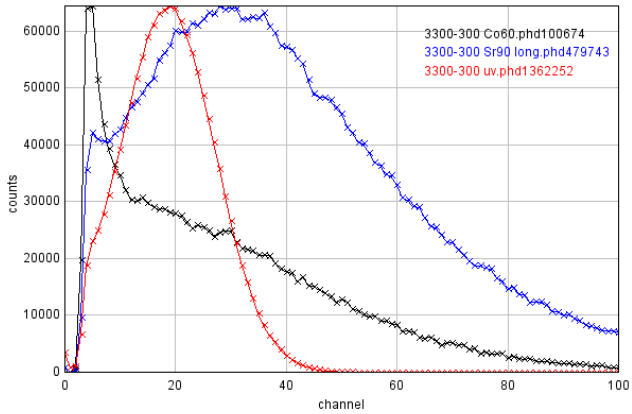

Fig. 12. Standard MCP pair (33mm, 12µm pore, 60:1 L/d, 12° bias) gain ~5 × 10^6, Pulse height spectra for UV, ^{60}Co gammas (2% detection efficiency) and ^{90}Sr ß (~24% efficiency).

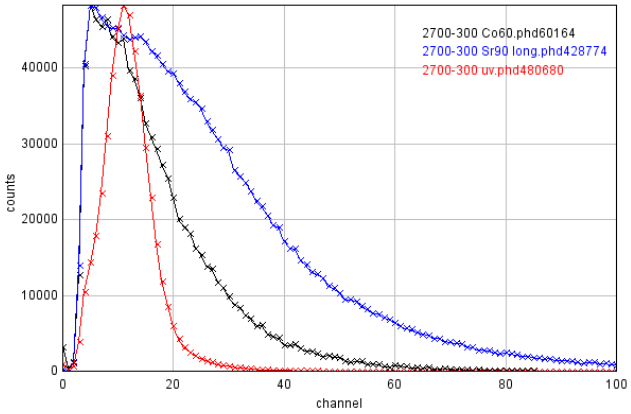

Fig. 13: ALD MCP pair (33mm, 20µm pore, 60:1 L/d, 8° bias) gain ~3 × 10^6, with MgO layer. Pulse height spectra for UV, ^{90}Sr ß (~27% detection efficiency) & ^{60}Co gammas (~0.8% efficiency).

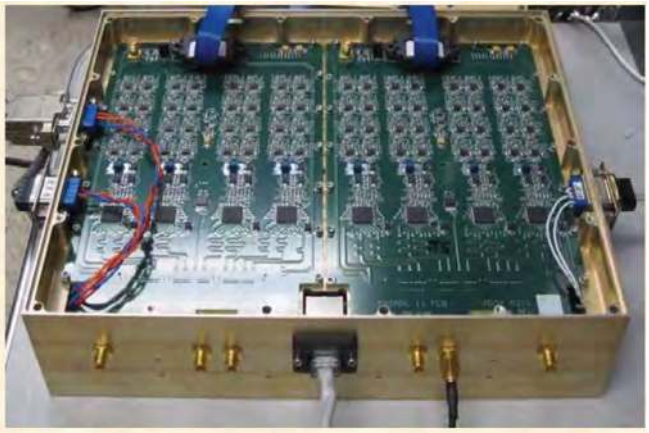

Figure 14. PXS-II cross strip anode position encoding electronics. Uses direct 50 MHz digitization of RD20 preamp signals and event centroiding firmware on a Xilinx Virtex-6 FPGA for ~5MHz rates.

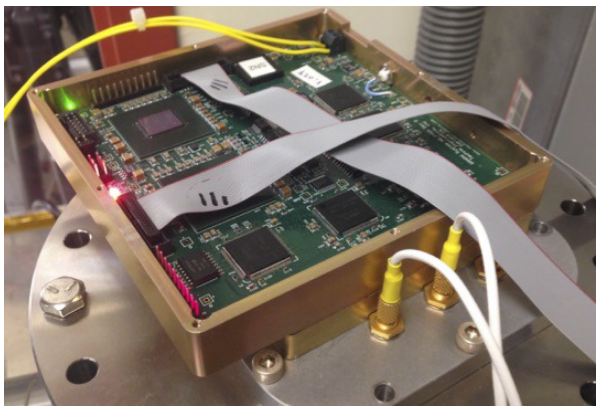

Figure 15. Prototype ASIC cross strip encoding electronics (CSAv3/ HalfGraph). The preamp has a 4x faster time constant than PXS-II, & is followed by gigasample/s sampling & storage arrays, & FPGA's for centroid algorithms at >5MHz rates.

4. CROSS STRIP ANODE EVENT POSITION ENCODING ELECTRONICS

In the existing PXS-II (Fig. 14) electronics scheme each strip on the anode is connected directly to a preamp input of a 32-channel the "Preshape32" ASIC[29,30]. The preamp outputs are shaped unipolar pulses of ~40 ns rise time, ~400 ns fall time and ~1200 electrons RMS noise. The parallel preamp outputs (128 × 128 for 100 mm XS, Fig. 3) are post amplified before being continuously digitized by 50 mega-sample per second 12-bit analog to digital converters. These digital samples are fed into an FPGA where they are digitally filtered to determine the event centroid for both X and Y axes. The events are then transferred to a downstream computer as an event list of X, Y, time and pulse height with up to 14 of bits of position binning in each axis. The PXS-II electronics, has achieved ~18 µm FWHM spatial resolution (~5 µm binning) on a 95 × 95 mm XS at rates up to 5 MHz with ~15% dead time. The PXS-II mass and power is not optimal for all space applications, so two application specific

Downloaded From: https://www.spiedigitallibrary.org/conference-proceedings-of-spie on 1/29/2018 Terms of Use: https://www.spiedigitallibrary.org/terms-of-use

integrated circuits (ASICs) called the CSAv3 and the HalfGRAPH are in development. These are designed to decrease the mass and power while improving the event throughput performance[21]. The 16 channel CSAv3 ASIC is a charge sensitive preamp with a 20 ns risetime and baseline return in less than 100 ns. The 16 channel HalfGRAPH ASIC samples the preamp waveform at 1 GHz and digitizes these analog samples with low power Wilkinson ADCs triggered by the preamp. Both these ASICs have been fabricated and integrated into a prototype system (Fig. 15) which has begun testing.

5. ATOMIC LAYER MCP CONFIGURATIONS AND IMAGING

The majority of applications utilize flat focal planes and thus flat MCPs. However, there are a substantial subset of missions where curved surface MCPs have been used[28,31], and this will also be the case for LUVOIR. C14 ALD MCPs have been curved to small radii (Fig. 16) and tested in pairs and triplets. The gain, background and sensitivity performance is essentially the same as their flat

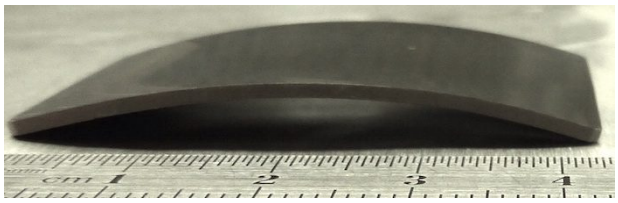

Figure 16. Cylindrically curved borosilicate-ALD MCP, 46 × 30mm, R = 75 mm with 20 µm pores, 60:1 L/d, 13° bias.
.

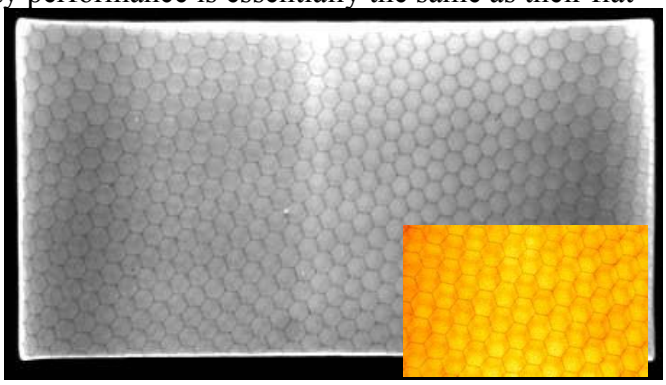

Figure 17. Image for 254nm illumination of the MCP type shown in Fig. 16, shows the hexagonal modulation of the image and the inset gain map. Modulation in both characteristics is of the order ~15%.

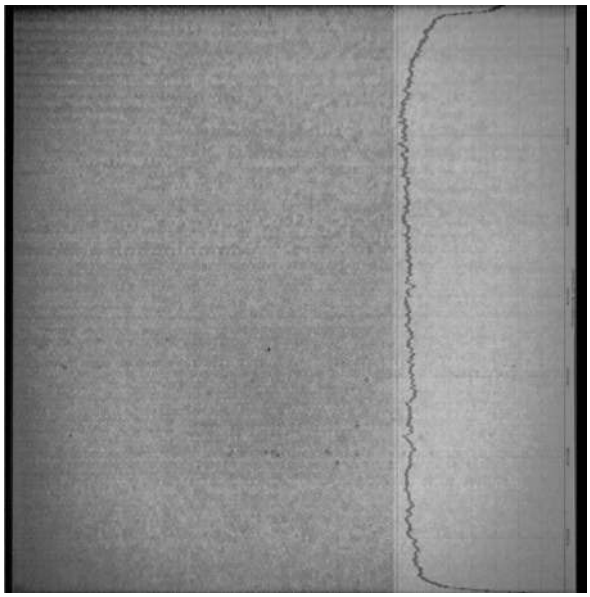

Figure 18. Average gain image for a pair of 200 mm square ALD MCPs with 20 µm pores, C5 substrate, 60:1 L/d, 8° bias, 254 nm UV, gain ~5 × $10^{6,}$ inset histogram shows gain is flat.

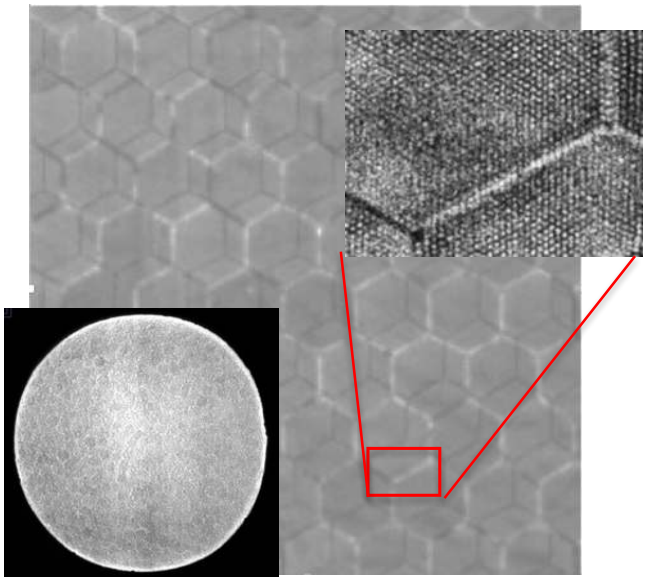

Figure 19. Image using 254 nm illumination for a pair of 100 mm square ALD MCPs (20 µm pore, borosilicate, 60:1 L/d, 8° bias). The 95 mm XS readout can resolve the pores (zoom). Inset – initial image for the 6µm pore 33mm ALD MCPs (pair).

Downloaded From: https://www.spiedigitallibrary.org/conference-proceedings-of-spie on 1/29/2018 Terms of Use: https://www.spiedigitallibrary.org/terms-of-use

counterparts. Imaging (Fig. 17) shows hexagonal modulation in the image and average gain map for both the top and bottom MCP of the stack. The level of the modulation is modest (~15%) and parallels the progressive improvements in physical construction for conventional MCPs. The thermal slumping technique used has been applied to MCPs as large as 125 mm. Additionally, the large 200 × 200 mm^2 flat ALD borosilicate MCPs are mechanically robust with gain (Fig. 18) and background (Fig. 11) performance that is uniform over the whole area. Examination of the imaging performance of the 20 µm pore MCPs in greater detail has been accomplished with a 10 × 10 cm^2 cross strip PXS-II readout detector system[11]. This shows that the MCP pores can be resolved (Fig. 19) and shows the bright/dark modulation effects of pore distortions at the multifiber boundaries (Fig. 5). Large 200 × 200 mm^2 ALD MCPs with 10 µm pores are currently in fabrication, and smaller 33 mm MCPs with 6 µm pores have been made and successfully tested (Fig. 19).

6.PHOTOCATHODE OPTIONS AND CHARACTERISTICS

The photocathode material and the detection of emitted photoelectrons by the MCP determine the quantum efficiency (QE) of an MCP sensor[5,7]. Bare MCPs have relatively poor QE, but the ALD MCPs show better EUV QE than even the best conventional MCPs (Fig. 20). Opaque alkali halides photocathodes are widely used for EUV/UV sensors (Figs. 21, 22), and semitransparent multialkali photocathodes for visible detectors. Alkali halide (CsI, KBr) opaque photocathodes on MCPs obtain high QE (~50% at ~110 nm) and have broad band sensitivity from 10 nm to 160 nm. Results for ALD MCPs coated with Alkali Halides give QEs comparable to the best conventional MCPs with photocathodes, however the ALD MCP bias angles are not yet optimized (8° or 13° vs 20° for conventional MCPs). New materials such as GaN are potential candidates to replace the traditional solar blind CsTe semitransparent photocathodes. We have achieved high QE (Fig. 23) for GaN on Al_2O_3 substrates and directly on early ALD MCPs[32] and have now begun investigation of opaque GaN on C14 ALD MCPs.

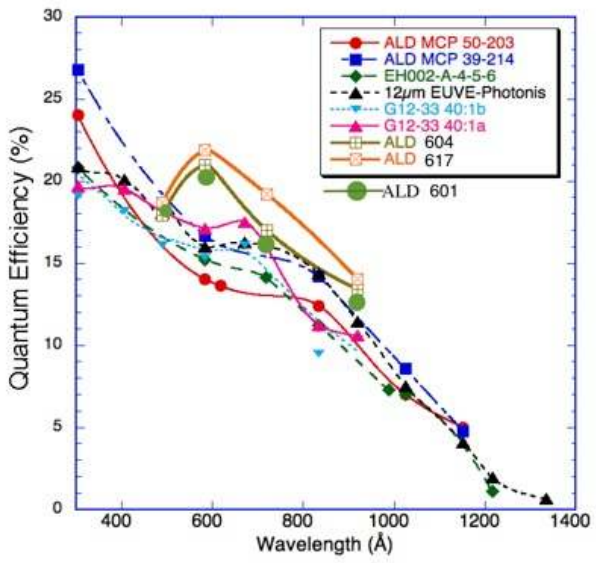

Figure 20. UV QE for bare ALD MCPs with 73% open area, Al_2O_3 or MgO emissive layers, 20 µm pores, 60:1 l/d, 13° bias, compared with the best conventional MCPs (12µm pore).

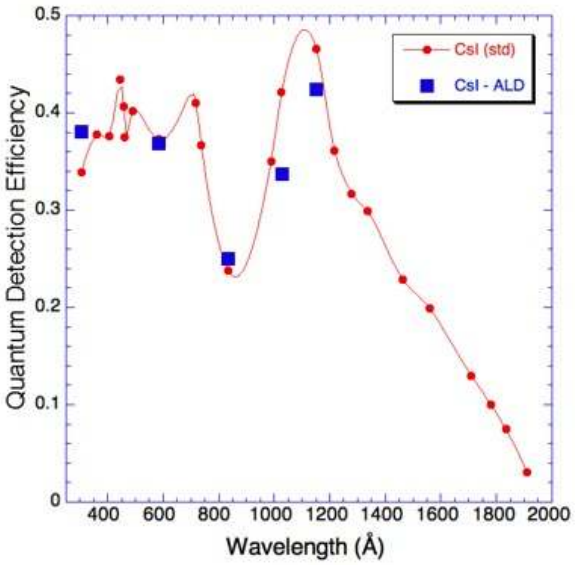

Figure 21. UV quantum efficiency for the best standard MCPs (12µm pore, 80:1 L/d, lead glass, 20° bias) coated with an opaque CsI photocathode. Also, UV QE for MgO ALD MCPs 20 µm pores, 60:1 l/d, 8° bias with opaque CsI cathode.

Downloaded From: https://www.spiedigitallibrary.org/conference-proceedings-of-spie on 1/29/2018 Terms of Use: https://www.spiedigitallibrary.org/terms-of-use

Traditional visible sensitive photocathodes like bialkali (Na_2KSb) have 30% peak at 350nm but also show high QE in the UV (Fig. 24)[33] that has not been previously utilized for UV sensors. We have made a number of large area (20 × 20 cm^2) bialkali semitransparent photocathodes[19] and have consistently achieved ~25% QE at 370 nm with good overall uniformity (±15%)[34]. Sealed tube bialkali cathode device lifetimes have improved using ALD coated MCPs[23]. Extending response to UV by using MgF_2 windows is relatively simple, and the large open area for ALD MCPs would enhance the QE. Alkali halides, or GaN, could be also applied to the MCP in the same device to boost FUV efficiency (Fig 25), and the red response of the bialkali can be minimized by using thin cathodes.

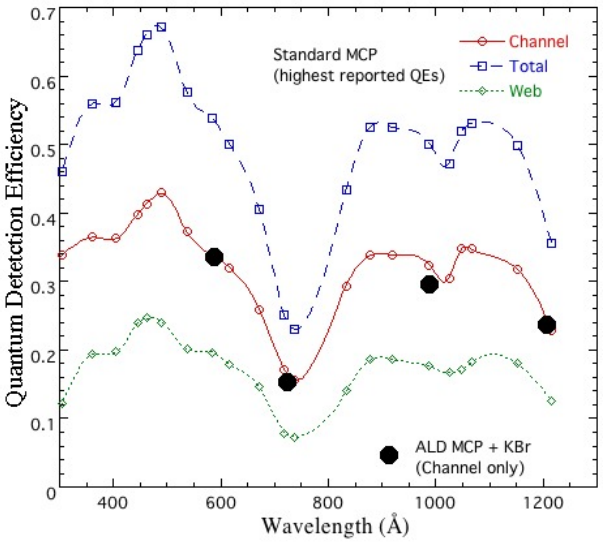

Figure 22. Quantum efficiency for a C5 MCP (20µm pore, 60:1 L/d, 13° bias, MgO ALD) with an opaque KBr cathode.

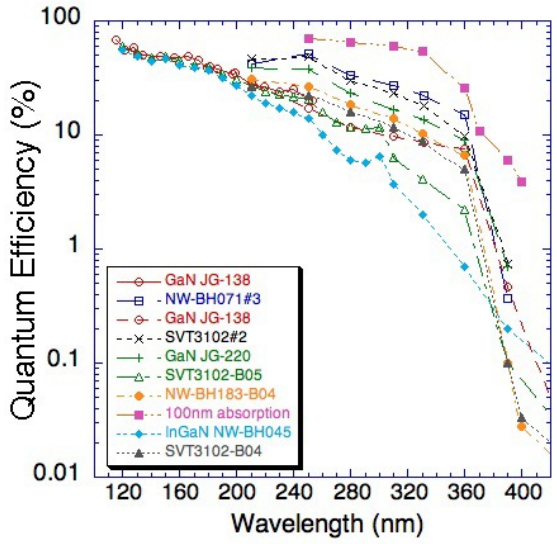

Figure 23. Quantum efficiency for different GaN(Mg) opaque photocathodes deposited onto sapphire substrates.

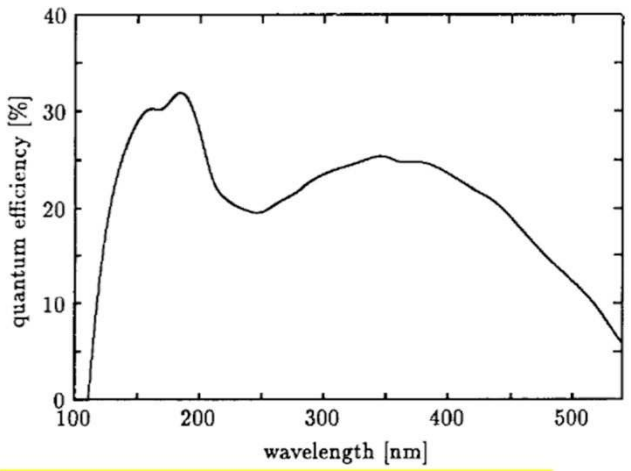

Figure 24. EMI 9426 photomultiplier bialkali photocathode UV response at ~200 nm shows a 30% peak (MgF_2 window)[33]. Similar results have been obtained in other PMTs[35] & tests[36].

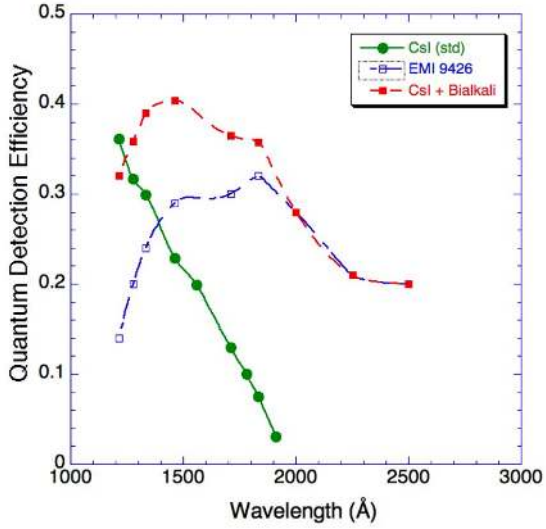

Figure 25. Comparison of semitransparent bialkali and opaque CsI UV efficiency. Both can be combined in a sealed tube MCP (predicted curve assumes 50% transparency for the bialkali).

7. DETECTOR IMPLEMENTATION

There are a large number of MCP based detector systems that have been used in astronomical, solar and planetary mission instruments[31,37,38]. Recent and pending implementations are beginning to

Downloaded From: https://www.spiedigitallibrary.org/conference-proceedings-of-spie on 1/29/2018 Terms of Use: https://www.spiedigitallibrary.org/terms-of-use

use the new ALD MCPs and cross strip readouts. Specific examples are the CHESS sub-orbital instrument[39] cross strip readout sensor, and the space station LITES ALD MCP detector[40]. There are other applications in other fields, including the LAPPD[13] (Fig. 26) sealed tube 200mm devices for high energy physics (Cherenkov) applications. Upcoming endeavors include the DEUCE 200 mm open face ALD MCP, cross delay line detector (Fig. 27) for a UV spectroscopy sub-orbital experiment. Other devices, such as a Planacon 50 mm (32 x 32 pad) sealed tube bialkali photocathode device with ALD MCPs (Fig. 28) and a 25 mm aperture sealed tube with ALD MCPs with an opaque GaN(Mg) photocathode and XDL readout have been made. These each test some of the elements desired in the LUVOIR baseline. Over a three-year test period, the photocathode in the Planacon has not degraded at all[23], outlining the low outgassing residuals for ALD MCPs. Over that same time period the GaN sealed tube shows no degradation of MCP gain[17], background or pulse height distributions.

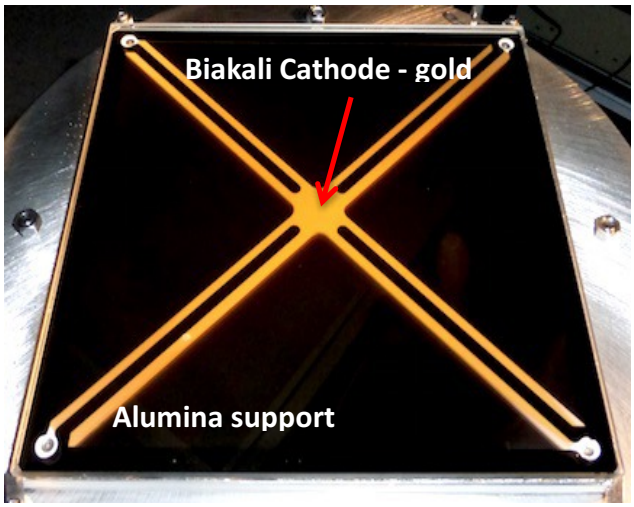

Figure 26. Sealed tube 200 x 200mm device using a pair of 200 mm square ALD MCPs (20 µm pore, borosilicate, 60:1 L/d, 8° bias). Inter-MCP 0.7 mm gap with 200 V bias.

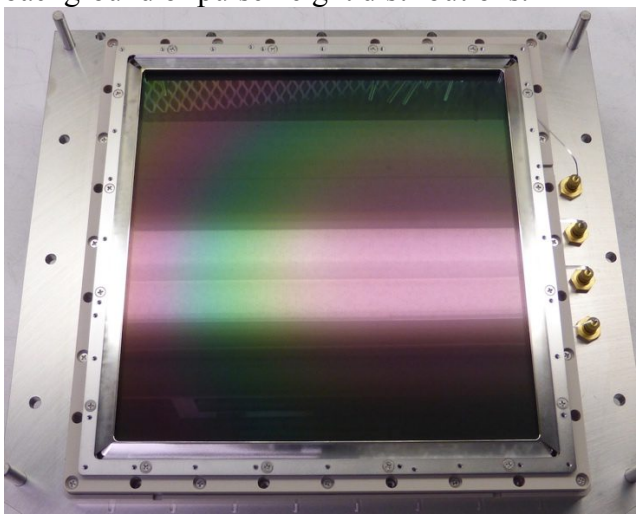

Figure 27. KBr photocathode deposited onto a 200 × 200 mm ALD MCP in a large detector with a cross delay line anode readout for sounding rocket UV spectroscopy[41].

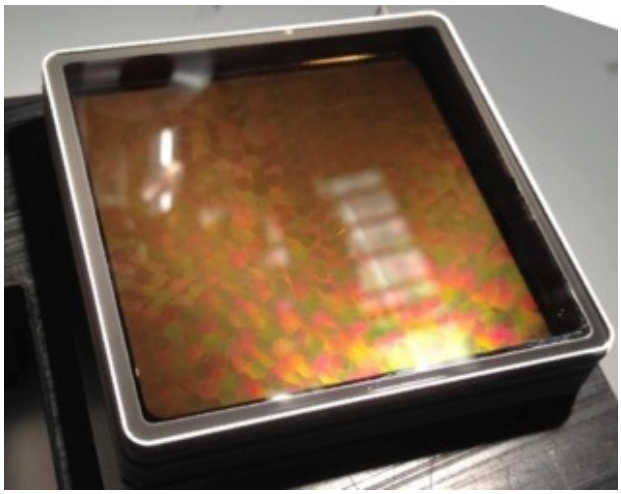

Figure 28. Planacon 50 mm sensor with a bialkali semitransparent photocathode and a pair of 53 mm, 10 µm pore, 60:1 L/d, 8° bias C5 ALD borosilicate MCPs, 32 × 32 anode pad array.

Figure 29. Sealed tube detector with 33 mm ALD MCPs and an opaque GaN photocathode deposited on the top MCP. (20 µm pore 60:1 L/d, 8° bias with Al_2O_3 ALD layer applied).

Key elements in the development of ALD MCPs and cross strip readouts for future missions are their large area scalability and significant reduction in background event rates in addition to robust

Downloaded From: https://www.spiedigitallibrary.org/conference-proceedings-of-spie on 1/29/2018 Terms of Use: https://www.spiedigitallibrary.org/terms-of-use

long term gain stability, and low outgassing rate after sealed tube processing. Also relevant is the ability to curve the MCPs to focal planes and reject in situ high energy background radiation. Important goals to achieve for LUVOIR/CETUS/HabEx include demonstrations of high throughput / high spatial resolution cross strip readouts and electronics for 200 mm formats using 10 μm pore ALD MCPs. Optimization of high efficiency / wide band photocathodes and hybrid cathodes with ALD MCPs in ≥100 mm sealed tubes is also an important step in realization of LUVOIR implementation.

ACKNOWLEDGEMENTS

We wish to thank J. Hull, J. Tedesco, R. Raffanti, Dr. G Varner, Dr. J. DeFazio and Photonis, and Dr. T. Cremer and the team at Incom Inc. for their contributions to this work. This work was supported by under NASA grants NNG11AD54G and NNX14AD34G.

REFERENCES

[1] Tremsin, A., Lebedev, G. V., Siegmund, O. H. W., Vallerga, J., McPhate, J. B., Hussain, Z., "High-resolution detection system for time-of-flight electron spectrometry," Nucl. Instr. Meth. Phys. Res. A **582**(1), 172–174 (2007).

[2] Siegmund, O. H. W., Welsh, B., Vallerga, J., Tremsin, A., McPhate, J., "High-performance microchannel plate imaging photon counters for spaceborne sensing," Proc. SPIE **6220**, 622004–622004–12 (2006).

[3] Tremsin, A., Siegmund, O. H. W., Vallerga, J., Hull, J. S., Abiad, R., "Cross-strip readouts for photon counting detectors with high spatial and temporal resolution," IEEE Trans. Nucl. Sci. **51**(4), 1707–1711 (2004).

[4] Siegmund, O. H. W., Jelinsky, P. N., Jelinsky, S. R., Stock, J. M., Hull, J. S., Doliber, D. L., Zaninovich, J., Tremsin, A., Kromer, K. E., "High-resolution cross delay line detectors for the GALEX mission," Proc. SPIE **3765**, 429–440 (1999).

[5] Siegmund, O. H. W., "Methods of vacuum ultraviolet physics," [Vacuum Ultraviolet Spectroscopy], D. L. Ederer and J. A. R. Samson, Eds., Academic Press (1998).

[6] Lampton, M., "The Microchannel Image Intensifier," Scientific American **245**(5), 62–71 (1981).

[7] Siegmund, O. H. W., Vallerga, J., Tremsin, A., "Characterizations of microchannel plate quantum efficiency," Proc. SPIE **5898**, 113–123 (2005).

[8] Siegmund, O. H. W., Vallerga, J., Welsh, B., McPhate, J., Rogers, D., "High Speed Optical Imaging Photon Counting Microchannel Plate Detectors for Astronomical and Space Sensing Applications," presented at Proceedings of the Advanced Maui Optical and Space Surveillance Technologies Conference, September 2009.

[9] Siegmund, O. H. W., Tremsin, A., Vallerga, J., Abiad, R., Hull, J., "High resolution cross strip anodes for photon counting detectors," Nucl. Instr. Meth. Phys. Res. A **504**(1-3), 177–181 (2003).

[10] Tremsin, A., Siegmund, O. H. W., Vallerga, J., Hull, J. S., "Novel high-resolution readout for UV and x-ray photon counting detectors with microchannel plates," Proc. SPIE **6276**, 16–11 (2006).

[11] Siegmund, O. H. W., Vallerga, J., Jelinsky, P., Michalet, X., Weiss, S., "Cross delay line detectors for high time resolution astronomical polarimetry and biological fluorescence imaging," IEEE Nucl Sci Conf R **1**, 448–452 (2005).

[12] Siegmund, O. H. W., Tremsin, A., Vallerga, J., Hull, J., "Cross strip imaging anodes for microchannel plate detectors," IEEE Trans. Nucl. Sci. **48**(3), 430–434 (2001).

[13] Ertley, C. D., Siegmund, O. H. W., Jelinsky, S. R., Tedesco, J., Minot, M. J., O'Mahony, A., Craven, C. A., Popecki, M., Lyashenko, A. V., et al., "Second generation large area microchannel plate flat panel phototubes," Proc. SPIE **9915**, 99152G–99152G–10 (2016).

[14] Ertley, C., Siegmund, O. H. W., Schwarz, J., Mane, A. U., Minot, M. J., O'Mahony, A., Craven, C. A., Popecki, M., "Characterization of borosilicate microchannel plates functionalized by atomic layer deposition," Proc. SPIE **9601**, 96010S–96010S–10 (2015).

[15] Siegmund, O. H. W., McPhate, J., Curtis, T., Jelinsky, S., Vallerga, J., Hull, J., Tedesco, J., "Ultraviolet imaging detectors for the GOLD mission," Proc. SPIE **9905**, 99050D–99050D–10 (2016).

[16] Siegmund, O. H. W., Vallerga, J., McPhate, J. B., Tremsin, A., "Next generation microchannel plate detector technologies for UV astronomy," Proc. SPIE **5488**, 789–800 (2004).

[17] Ertley, C., Siegmund, O. H. W., Tremsin, A., Hull, J., O'Mahony, A., Minot, M., Craven, C., "Microchannel

Downloaded From: https://www.spiedigitallibrary.org/conference-proceedings-of-spie on 1/29/2018 Terms of Use: https://www.spiedigitallibrary.org/terms-of-use

Plate Imaging Detectors for High Dynamic Range Applications," IEEE Trans. Nucl. Sci. **PP**(99), (2017).
[18] Michalet, X., Colyer, R. A., Scalia, G., Weiss, S., Siegmund, O. H. W., Tremsin, A., Vallerga, J., Villa, F., Guerrieri, F., et al., "New photon-counting detectors for single-molecule fluorescence spectroscopy and imaging," Proc. SPIE **8033**, 803316 (2011).
[19] Siegmund, O. H. W., McPhate, J., Frisch, H., Elam, J., Mane, A., Wagner, R., Varner, G., "Large Area Flat Panel Imaging Detectors for Astronomy and Night Time Sensing," presented at Proceedings of the Advanced Maui Optical and Space Surveillance Technologies Conference, September 2013.
[20] Tremsin, A., Shinohara, T., Kai, T., Ooi, M., Kamiyama, T., Kiyanagi, Y., Shiota, Y., McPhate, J. B., Vallerga, J., et al., "Neutron resonance transmission spectroscopy with high spatial and energy resolution at the J-PARC pulsed neutron source," Nucl. Instr. Meth. Phys. Res. A **746**, 47–58 (2014).
[21] Vallerga, J., McPhate, J., Tremsin, A., Siegmund, O. H. W., Raffanti, R., Cumming, H., Seljak, A., Virta, V., Varner, G., "Development of a flight qualified 100 x 100 mm MCP UV detector using advanced cross strip anodes and associated ASIC electronics," Proc. SPIE **9905**, 99053F–99053F–12 (2016).
[22] O'Mahony, A., Craven, C. A., Minot, M. J., Popecki, M. A., Renaud, J. M., Bennis, D. C., Bond, J. L., Stochaj, M. E., Foley, M. R., et al., "Atomic layer deposition of alternative glass microchannel plates," J. Vac. Sci. Technol. A **34**(1), 01A128 (2016).
[23] Lehmann, A., Britting, A., Eyrich, W., Uhlig, F., Dzhygadlo, R., Gerhardt, A., Götzen, K., Höhler, R., Kalicy, G., et al., "Improved lifetime of microchannel-plate PMTs," Nucl. Instr. Meth. Phys. Res. A **766**, 138–144 (2014).
[24] Siegmund, O. H. W., "Preconditioning of Microchannel Plate Stacks," Proc. SPIE **1072**, 111–118 (1989).
[25] Siegmund, O. H. W., Richner, N., Gunjala, G., McPhate, J. B., Tremsin, A., Frisch, H. J., Elam, J., Mane, A., Wagner, R., et al., "Performance characteristics of atomic layer functionalized microchannel plates," Proc. SPIE **8859**, 88590Y (2013).
[26] Jokela, S. J., Veryovkin, I. V., Zinovev, A. V., Elam, J. W., Mane, A. U., Peng, Q., Insepov, Z., "Secondary Electron Yield of Emissive Materials for Large-Area Micro-Channel Plate Detectors: Surface Composition and Film Thickness Dependencies," Physics Procedia **37**, 740–747 (2012).
[27] Siegmund, O. H. W., Fujiwara, K., Hemphill, R., Jelinsky, S. R., McPhate, J. B., Tremsin, A., Vallerga, J., Frisch, H. J., Elam, J., et al., "Advances in microchannel plates and photocathodes for ultraviolet photon counting detectors," presented at Proc. SPIE **8145**, 81450J–81450J–12 (2011).
[28] Hurwitz, M., Bowyer, S., Bristol, R., Van Dyke Dixon, W., Dupuis, J., Edelstein, J., Jelinsky, P., Sasseen, T. P., Siegmund, O. H. W., "Far-Ultraviolet Performance of the Berkeley Spectrograph duringthe ORFEUS-SPAS II Mission," ApJ **500**(1), L1–L7, IOP Publishing (1998).
[29] Vallerga, J., Raffanti, R., Cooney, M., Cumming, H., Varner, G., Seljak, A., "Cross strip anode readouts for large format, photon counting microchannel plate detectors: developing flight qualified prototypes of the detector and electronics," Proc. SPIE **9144**, 91443J (2014).
[30] Vallerga, J., Raffanti, R., Tremsin, A., Siegmund, O. H. W., McPhate, J., Varner, G., "Large-format high-spatial resolution cross-strip readout MCP detectors for UV astronomy," Proc. SPIE **7732**, 773203 (2010).
[31] Gladstone, R., Versteeg, M., Greathouse, T. K., Hue, V., Davis, M., Gerard, J.-C., Grodent, D., Bonfond, B., "Juno Ultraviolet Spectrograph (Juno-UVS) Observations of Jupiter during Approach," AAS **48**, #402.02 (2016).
[32] Tremsin, A., Hull, J. S., Siegmund, O. H. W., McPhate, J. B., Vallerga, J., Dabiran, A. M., Mane, A., Elam, J., "Opaque gallium nitride photocathodes in UV imaging detectors with microchannel plates," Proc. SPIE **8859**, 88590X (2013).
[33] Dorenbos, P., de Haas, J. T. M., Visser, R., van Eijk, C. W. E., Hollander, R. W., "Quantum efficiencies of several VUV-sensitive photomultiplier tubes," Nucl. Instr. Meth. Phys. Res. A **325**(1), 367–369 (1993).
[34] Siegmund, O. H. W., McPhate, J. B., Jelinsky, S. R., Vallerga, J., Tremsin, A., Hemphill, R., Frisch, H. J., Wagner, R. G., Elam, J., et al., "Large Area Microchannel Plate Imaging Event Counting Detectors With Sub-Nanosecond Timing," IEEE Trans. Nucl. Sci. **60**(2), 923–931 (2013).
[35] Araujo, H. M., Chepel, V. Y., Lopes, M. I., van der Marel, J., Marques, R. F., Policarpo, A. J. P. L., "Study of bialkali photocathodes below room temperature in the UV/VUV region," IEEE Trans. Nucl. Sci. **45**(3), 542–549 (1998).
[36] Xie, J., "Photocathodes with VUV-UV-Vis full range response for fast timing and imaging applications," presented at the International Conference on High Energy Physics, 5 August 2016.
[37] Retherford, K. D., Greathouse, T. K., Gladstone, G. R., Hendrix, A. R., Mandt, K. E., Egan, A. F., Kaufmann,

Downloaded From: https://www.spiedigitallibrary.org/conference-proceedings-of-spie on 1/29/2018 Terms of Use: https://www.spiedigitallibrary.org/terms-of-use

D. E., Hayne, P. O., Bullock, M. A., et al., "The Far-UV Albedo of the Moon as a Probe of the Lunar Cryosphere: LRO Lyman Alpha Mapping Project (LAMP) Latest Results," 46th Lunar and Planetary Science Conference **46**, 2213 (2015).

[38] Gladstone, G. R., Stern, S. A., Weaver, H. A., Young, L. A., Ennico, K. A., Olkin, C. B., Cheng, A. F., Greathouse, T. K., Hinson, D. P., et al., "New Horizons Observations of the Atmospheres of Pluto and Charon," AAS **47**, 100.05 (2015).

[39] Hoadley, K., France, K., Kruczek, N., Fleming, B., Nell, N., Kane, R., Swanson, J., Green, J., Erickson, N., et al., "The Re-Flight of the Colorado High-Resolution Echelle Stellar Spectrograph (CHESS): Improvements, Calibrations, and Post-Flight Results," Proc. SPIE **9905**, 99052V–99052V–19 (2016).

[40] Stephan, A. W., Budzien, S. A., Chakrabarti, S., "LITES and GROUP-C Mission Update: Ionosphere and Thermosphere Sensing from the ISS," AGU (2016).

[41] Green, J. C., "Dual-channel Extreme Ultraviolet Continuum Spectrograph (DEUCE)," https://sites.wff.nasa.gov/code810/news/story209.html (25 August 2017).

Downloaded From: https://www.spiedigitallibrary.org/conference-proceedings-of-spie on 1/29/2018 Terms of Use: https://www.spiedigitallibrary.org/terms-of-use